Unmanned Systems, Vol. 14, No. 4 (2026) 775–786

DOI: 10.1142/S2301385026500184

Unmanned Systems
https://www.worldscientific.com/worldscinet/us

A Novel Fixed Time Formation for Unmanned Ground Vehicles Under Communication Denial Conditions: Relative Information Control Method

Xinhai Zhuang [*], Jingyi Liu [*,‡], Hengyu Li [*], Yueying Wang [*], Jun Luo [*,†]

[*]School of Mechatronic Engineering and Automation,
Shanghai University, Shanghai 200444, P. R. China

[†]State Key Laboratory of Mechanical Transmission for Advanced Equipment,
Chongqing University, Chongqing 400044, P. R. China

Communication limitations and energy consumption are the two core challenges in the field of Unmanned Ground Vehicles (UGVs) formation control. To address these issues, this paper proposes a new fixed-time formation control strategy (FTFCS), particularly suitable for communication denial environments. The proposed strategy first utilizes onboard sensors to collect relative position information enabling the reconstruction of the position of the leader. Subsequently, based on this information, a high gain observer is constructed to achieve real-time estimation of the leader's velocity. Furthermore, considering the perceptual constraint range and collision avoidance requirements of UGVs, a novel FTFCS is designed by integrating the tanh-function and prescribed performance control (PPC). This approach effectively mitigates the inherent oscillations and high energy consumption issues associated with traditional FTFCS, resulting in a 30% reduction in energy consumption. Finally, simulation results validate the effectiveness of the proposed control strategy.

Keywords: Fixed-time control; unmanned ground vehicles (UGV); prescribed performance; collision avoidance; connectivity maintenance.

1. Introduction

Unmanned ground vehicles (UGVs) have seen significant development globally over the past few years, owing to their exceptional performance in a variety of applications. Particularly, their capacity to execute high-risk tasks in extreme conditions, where human presence is hazardous or infeasible, has rendered UGVs increasingly vital for intelligence gathering, resource surveying, and military operations [1–4]. Despite these advancements, UGVs remain vulnerable to communication disruptions caused by adverse weather conditions or enemy information warfare activities. Such disruptions can impede UGVs' ability to obtain or utilize precise positional and directional data from surrounding vehicles, potentially leading to formation breakdowns. Consequently, achieving high-precision formations under constrained communication resources presents a formidable challenge that this research aims to address.

There has been some previous research reported regarding the above-mentioned formation problem. Briefly, there are three main types in terms of formation structure: behavior methods [5], virtual structure methods [6], and leader follower (LF) methods [7, 8]. However, it is worth noting that the LF method exhibits several advantageous characteristics, including flexible formation and low computational complexity, which make it particularly effective in handling large-scale robot swarms. Leveraging these advantages, significant research progress has been made in this area. Wang *et al.* [9] designed an adaptive LF formation tracking controller to address the potential slippage problem of robots on low-adhesion roads such as ice, sand, or mud, effectively improving the stability and robustness of the formations in complex environments. In [10], an adaptive PID formation control strategy was proposed to solve the cluster control problem of unknown leader robot speeds in the leader follower framework, further improving robustness.

Received 10 December 2024; Revised 19 February 2025; Accepted 21 February 2025; Published 5 May 2025. This paper was recommended for publication in its revised form by editorial board member, Lu Liu.
Email Addresses: [‡]liujingyi@shu.edu.cn
[‡]Corresponding author.

Li *et al*. [11] proposed an adaptive fuzzy formation control method to address the issue of possible actuator failures in UGVs. In [12], a disturbance observation method based on a predictor was proposed for the formation control problem with unknown disturbances. It is worth noting that the aforementioned research results primarily address unknown disturbances, actuator failures, and sideslip issues. However, all the above results are obtained with time converging to infinity, which means that the tracking error cannot converge to the equilibrium point or its neighborhood according to practical needs. This poses a challenge in practical applications, so it is crucial to design a time-controllable formation control controller.

From a practical perspective, how to improve the real-time performance and efficiency of the system, as well as more efficient and precise control, has always been a hot topic in the field of control. Among many research results, finite-time control has garnered extensive scholarly attention due to its superior convergence characteristics compared to traditional control methods, with substantial achievements reported in recent report. For instance, a fast finite-time control method was developed in [13] for nonlinear systems with full state constraints. The methodology was extended to nonlinear multi-agents, encompassing trajectory tracking and formation control of UGVs. Li *et al*. [14] proposed an event-triggered finite-time formation controller applicable to UGVs subject to multiple constraints. The work in [15] investigated visual tracking control for UGV formation systems with uncertain dynamic models and visibility constraints. Nevertheless, a critical limitation persists: The convergence time of these methods exhibits extreme sensitivity to initial conditions, imposing stringent requirements that hinder practical implementation. This strict requirement creates difficulties for practical applications. To address this challenge, [16] introduced a fixed-time control framework capable of decoupling convergence time from initial states, thereby overcoming the aforementioned limitation. Building on this, Dai *et al*. [17] developed a fixed-time control strategy tailored for UGVs operating under field-of-view constraints. These theoretical advances have subsequently been adapted to diverse practical systems, including robotic manipulators [18], quadrotor UAVs [19], and unmanned surface vehicles (USVs) [20]. Notably, while existing research has achieved remarkable progress in convergence rate optimization, it predominantly overlooks the critical issue of high-amplitude control signal oscillations. In practical control systems, particularly in robotics, such oscillations may accelerate actuator wear, compromise operational lifespan, and potentially induce system instability challenges that demand urgent attention for real-world deployment.

Another noteworthy problem is that, despite significant advancements in on-board sensor technology in the domains of autonomous driving and robotics, the limitation of their sensing range remains a problem that cannot be overlooked. Achieving formation control and collision avoidance within a limited communication range is a longstanding theoretical and practical challenge in the field. To address this challenge, researchers have proposed a variety of solutions. Li *et al*. [21] proposed a formation controller based on LF for UGVs, which combines a generalized obstacle Lyapunov function and a performance function to maintain connectivity and collision avoidance (CA). In [22], the authors solved formation control problem for USV with unknown dynamics based on time-tuned functions and nonlinear transformations and neural network control. Dai *et al*. [23] proposed an adaptive formation controller based on LF, which integrates tan-obstacle function and prescribed performance control (PPC) for the purpose of maintaining connectivity and collision avoidance. Although research on maintaining connectivity and collision avoidance has garnered considerable attention, it remains an urgent issue to solve how to complete the formation within a fixed time and minimize energy loss using only on-board sensors under communication constraints.

This paper investigates the problem of formation control of UGVs under communication denial situation, which presents a significant challenge. In the scenario where UGVs cannot communicate, followers cannot access the position information and velocity information of the leaders. Consequently, this paper first reconstructs the leader's position information based on on date from the vehicle and sensors, and then real-time estimation of the velocity information by constructing a high-gain observer. Addressing the dual requirements of maintaining communication connectivity and collision avoidance (CA), this paper introduces strategies of PPC and obstacle functions. The integration of these two techniques not only ensures the connectivity of UGV formations in dynamic environments but also effectively mitigates potential collision risks. More importantly, the implementation of these strategies significantly enhances the system's transient performance, enabling UGV formations to respond swiftly to unexpected situations. Additionally, considering the issue of high amplitude oscillations in control signals that may be induced by traditional fixed-time control, this paper ingeniously utilizes the saturation properties of the tanh function to design a novel fixed-time controller. This controller not only effectively reduces the oscillation amplitude of the control signal and improves system stability but also aids in conserving energy. The contributions of this paper are outlined as:

(1) Unlike existing research results [11, 14, 15, 24], the results presented in this paper were achieved under communication denial conditions. In cases of communication denial, this paper reconstructs the leader's position information using data obtained from onboard

sensors and designs a high-gain observer to realize real-time estimation of the leader's velocity information.

(2) Compared with relevant studies in existing literature [17, 25–27], a novel fixed time controller has been designed, which significantly reduces the problems of excessive control signal amplitude and energy consumption during system execution while ensuring control performance.

(3) In order to solve the multi-constraint problem, this paper adopts the generalized barrier Lyapunov function to design the controller, which both solves the asymmetric visibility constraint problem and avoids the collision between UGVs.

2. Problem Formation and Preliminaries

2.1. *Fixed-time stability and preliminaries*

Lemma 1. ([17]). *If there exists a continuous radially unbounded and positive definite function* $V(x)$ *such that*

$$\dot{V}(x) \leq -\hbar_1 V^p(x) - \hbar_2 V^q(x) \tag{1}$$

for constants $\hbar_1 > 0, \hbar_2 > 0, p > 1, 0 < q < 1$, *then system is fixed-time stable and the settling time function* T *can be estimated by* $T \leq T_{\text{MAX}} = \frac{1}{\hbar_1(p-1)} + \frac{1}{\hbar_2(1-q)}$.

2.2. *Formation control for maintaining connectivity and avoiding collisions*

In *L-F* framework, let the index set $M = \{0, 1, \ldots, N\}, l, f \in M$. R_l as leader, provide reference signals for followers R_f. R_f acts as a follower to detect and follow the leader R_l. The kinematic of the ith UGV is described by

$$\begin{aligned} \dot{x}_i &= v_i \cos\psi_i, \\ \dot{y}_i &= v_i \sin\psi_i, \\ \dot{\psi}_i &= w_i, \end{aligned} \tag{2}$$

where $\boldsymbol{q_i} = [x_i, y_i, \psi_i]^T$ denotes ith UGV position coordinates and heading angle, respectively. $\boldsymbol{v_i} = [v_i, w_i]^T$ denotes the linear and angular velocities that are used as the control inputs.

According to the LF method shown in Fig. 1, the relative distance d_f and angle ϑ_f are defined

$$\begin{aligned} d_f &= \left((x_f - x_l)^2 + (y_f - y_l)^2\right)^{\frac{1}{2}}, \\ \vartheta_f &= a\tan 2(\dot{y}_f, \dot{x}_f), \end{aligned} \tag{3}$$

$$\begin{bmatrix} \dot{x}_f \\ \dot{y}_f \end{bmatrix} = \begin{bmatrix} \cos\psi_f & \sin\psi_f \\ -\sin\psi_f & \cos\psi_f \end{bmatrix} \begin{bmatrix} x_l - x_f \\ y_l - y_f \end{bmatrix}. \tag{4}$$

Due to the lack of network communication between GUVs, information exchange can only be obtained through

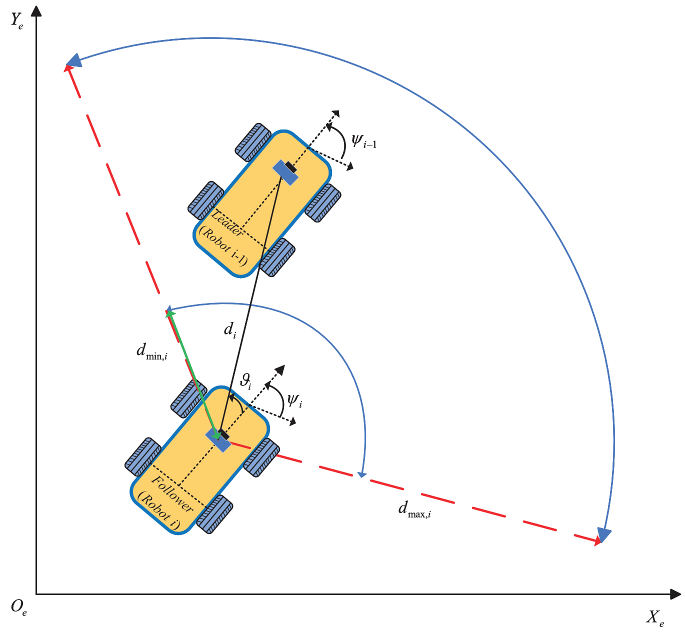

Fig. 1. Multirobot LF formation with multiple constraints.

onboard sensors. Additionally, it is assumed that the onboard sensors are not omnidirectional; they are fixed and have constraints on perception distance and field of view. Therefore, to meet the design requirements of subsequent controllers, we introduce the following constraint conditions.

$$0 < d_{\min,f} < d_f < d_{\max,f}, \tag{5}$$

$$-\vartheta_{\max,f} < \vartheta_f < \vartheta_{\max,f}, \tag{6}$$

where $d_{\max,f}$ and $\vartheta_{\max,f}$ are the maximum perceptual distance and angle, respectively. $d_{\min,f}$ denotes the minimum safe distance to collision avoidance with $0 < d_{\min,f} < d_{\max,f}, \vartheta_{\max,f} < \pi/2$.

Remark 1. (i) Collision Avoidance (CA): To ensure safety and CA, the distance maintained between UGVs must be greater than a specified threshold: $d_f(t) > d_{min,f} > 0$. (ii) Limited Perceptual Ability (LPA): The LPA can be divided into two main aspects. Firstly, there is distance perception. As we know, binocular vision or other perception devices have certain line of sight limitations, so corresponding constraints need to be set, $d_f(t) < d_{\max,f}$. Secondly, there is a limitation on the perception field of view. For binocular vision systems, their effective perception area is often fan-shaped, so specific constraints $|\vartheta_f| < \vartheta_{\max,f} < \frac{\pi}{2}$ need to be introduced to ensure the achievement of control objectives.

It is obvious that due to sensor limitations, the UGV is constrained to move within a fan-shaped area. Furthermore, the time-varying formation tracking errors are defined

$$e_{df} = d_f - d_f^*, \tag{7}$$

$$e_{\vartheta f} = \vartheta_f - \vartheta_f^*, \tag{8}$$

where d_f^* and ϑ_f^* are the expected distance and angle to be designed, with $d_{\min,f} < d_f^* < d_{\max,f}$ and $-\vartheta_{\min,f} < \vartheta_f^* < \vartheta_{\max,f}$, substituting (7) and (8) to (5) and (6) yield

$$d_{\min,f} - d_f^* < e_{df} < d_{\max,f} - d_f^*, \tag{9}$$

$$-\vartheta_{\max,f} - \vartheta_f^* < e_{\vartheta f} < \vartheta_{\max,f} - \vartheta_f^*. \tag{10}$$

Generally speaking, the transient and steady-state performance of tracking errors are considered key indicators for evaluating the quality of control systems. The PPC strategy facilitates the pre-definition of a funnel-shaped performance envelope during the controller design phase, ensuring that tracking errors evolve gradually in this envelope to meet established transient and steady-state performance requirements. Therefore, (9) and (10) can be rewritten as a constraint with performance function

$$-\chi_{df}\beta_{df} < e_{df} < \beta_{df}, \quad \forall t \geq 0, \ \ f \in \mathbb{N}, \tag{11}$$

$$-\chi_{\vartheta f}\beta_{\vartheta f} < e_{\vartheta f} < \beta_{\vartheta f}, \quad \forall t \geq 0, \ \ f \in \mathbb{N}, \tag{12}$$

where $\chi_{df} = \frac{d_{\min,f} - d_f^*}{d_f^* - d_{\max,f}}$, $\chi_{\vartheta f} = \frac{\vartheta_{\max,f} + \vartheta_f^*}{\vartheta_{\max,f} - \vartheta_f^*}$ $\chi_{jf} > 0$, $j = d, \vartheta$, and β_{jf} is a performance function that can be described as

$$\beta_{jf} = (\beta_{jf,0} - \beta_{jf,\infty})\exp(-\nu_{jf}t) + \beta_{jf,\infty}, \quad j = d, \vartheta, \tag{13}$$

where $\beta_{df,0} = d_{\max,f} - d_f^*$, $\beta_{\vartheta f,0} = \vartheta_{\max,f} - \vartheta_f^*$, and $\beta_{jf,\infty}$ are steady-state performance boundaries, and ν_{jf} is a positive constant to be designed. To achieve normalization of errors, the following error transformations are defined:

$$\zeta_{jf}(t) = \frac{e_{jf}}{\beta_{jf}}, \quad j = d, \vartheta. \tag{14}$$

In order to deal with the time-varying and asymmetry constraints, a new barrier function is introduced

$$B_{jf} = \frac{\bar{\zeta}_{jf}\underline{\zeta}_{jf}\zeta_{jf}}{(\bar{\zeta}_{jf} - \zeta_{jf})(\zeta_{jf} + \underline{\zeta}_{jf})}, \quad j = d, \vartheta \tag{15}$$

then, according to (11), (12) and (14) yield

$$-\chi_{jf} < \zeta_{jf}(t) < 1, \quad j = d, \vartheta. \tag{16}$$

Based on the above transformation, it is evident that when constraint (16) is met, constraints (11) and (12) are ensured to be met, thereby fulfilling constraints (5) and (6).

Formation Control Objective:

(1) The formation error e_{df} and $e_{\vartheta f}$ can converge to the neighborhood near zero in fixed time.

(2) Maintaining connectivity and LOS constraints throughout the entire formation process will not be violated.

3. Main Results

In this section, we not only reconstruct the leader's position information based on the onboard sensors, but also estimate the leader's velocity information in real time by constructing an observer, and ultimately design a novel fixed-time formation controller. The following is the specific design process.

3.1. *Reconstruction of leader position and design of high gain observer*

Due to the consideration of the formation control problem in the absence of communication between UGVs, it is necessary to estimate the position and velocity information of the corresponding leader.

By differentiating Eqs. (7) and (8), and based on Eq. (2), one can derive

$$\begin{aligned} \dot{e}_{df} &= -v_f \cos\vartheta_f + \dot{p}_l^T \Gamma_{1f}, \\ \dot{e}_{\vartheta f} &= \frac{1}{d_f}(v_f \sin\vartheta_f + \dot{p}_l^T \Gamma_{2f}) - w_f \end{aligned} \tag{17}$$

with $\dot{p}_l = [\dot{x}_l, \dot{y}_l]$, $\Gamma_{1f} = [\cos(\psi_f + \vartheta_f), \sin(\psi_f + \vartheta_f)]^T$ and $\Gamma_{2f} = [-\sin(\psi_f + \vartheta_f), \cos(\psi_f + \vartheta_f)]^T$.

It can be inferred that the leader's position p and velocity information $\dot{p}$ are unknown. Therefore, to achieve the controller design, it is necessary to reconstruct the position and estimate velocity information. Below is the specific design process.

3.1.1. *Reconstructing the position of leaders*

In this paper, we first reconstruct the leader's position information p_l from the available information.

$$\begin{aligned} x_l - x_f &= d_f \cos(\psi_f + \vartheta_f), \\ y_l - y_f &= d_f \sin(\psi_f + \vartheta_f) \end{aligned} \tag{18}$$

which gives

$$\begin{aligned} x_l &= x_f + d_f \cos(\psi_f + \vartheta_f), \\ y_l &= y_f + d_f \sin(\psi_f + \vartheta_f). \end{aligned} \tag{19}$$

From Eq. (19), we can infer that the leader's position information can be reconstructed by utilizing the follower's position and angle, as well as the relative distance and angle information obtained through onboard sensors. Next, we use a high gain observer to estimate $\dot{p}_l$.

3.1.2. *Design of high gain observer*

Let us consider the following linear system

$$\begin{cases}\varepsilon_f \dot{\eta}_{1f} = \eta_{2f}, \\ \varepsilon_f \dot{\eta}_{2f} = -\mu_f \eta_{2f} - \eta_{1f} + p_l,\end{cases} \tag{20}$$

where $\eta_{1f} = [\eta_{1,1f}, \eta_{1,2f}]^T$ and $\eta_{2f} = [\eta_{2,1f}, \eta_{2,2f}]^T$ are the system (20) states, the design parameter ε_f is a small positive constant, and the design parameter μ_f is chosen such that the polynomial $s^2 + \mu_f s + 1$ is Hurwitz. Then, according to (20), one has

$$\frac{\eta_{2f}}{\varepsilon_f} - \dot{p}_l = -\varepsilon_f \ddot{\Upsilon}_f, \tag{21}$$

where $\Upsilon_f = \eta_{2f} + \mu_f \eta_{1f}$, the term η_{2f}/ε_f in (21) can be employed to estimate $\dot{p}_l$, with estimate error $\varepsilon_f \ddot{\Upsilon}_f$, where $||\ddot{\Upsilon}_f|| < h_l$, being an unknown constant. i.e. the estimate error could be made arbitrary small by choosing small enough design parameters ε_f. The detailed proof can be found in [28].

3.2. ***Design of fixed time formation controller***

By differentiating (14) and combining (17), one gets

$$\dot{\zeta}_{df} = \frac{\Lambda_{df}(\zeta_{df})}{B_{df}(\zeta_{df})} \cdot \left[\frac{1}{\beta_{df}}(-v_f \cos\vartheta_f + \dot{p}_l^T \Gamma_{1f}) - \frac{\dot{\beta}_{df} e_{df}}{\beta_{df}^2}\right], \tag{22}$$

$$\dot{\zeta}_{\vartheta f} = \frac{\Lambda_{\vartheta f}(\zeta_{\vartheta f})}{B_{\vartheta f}(\zeta_{\vartheta f})} \cdot \left[\frac{1}{\beta_{\vartheta f}}\left(\frac{1}{d_f}(v_f \sin\vartheta_f + \dot{p}_l^T \Gamma_{2f}) - w_f\right)\right]. \tag{23}$$

In order to achieve fixed time formation control and minimize control, a novel FTFCS is proposed as

$$v_f = \alpha_{vf} \tanh\left(\frac{\alpha_{vf} \Lambda_{df} \cos(\vartheta_f)}{\beta_{df} \aleph}\right), \tag{24}$$

$$w_f = \alpha_{wf} \tanh\left(\frac{\alpha_{wf} \Lambda_{\vartheta f}}{\beta_{\vartheta f} \aleph}\right), \tag{25}$$

where

$$\alpha_{vf} = \frac{1}{\cos\vartheta_f}\left[\frac{g_{df}\beta_{df}\bar{\zeta}_{df}^2 \underline{\zeta}_{df}^2 \zeta_{df}}{(\bar{\zeta}_{df} - \zeta_{df})(\zeta_{df} + \underline{\zeta}_{df})} + \frac{\eta_{2f}^T \Gamma_{1f}}{\varepsilon_f} - \frac{\dot{\beta}_{df} e_{df}}{\beta_{df}} + \hat{h}_l \tanh\left(\frac{\Lambda_{df}\hat{h}_l}{\beta_{df}\sigma_f}\right)\right], \tag{26}$$

$$\alpha_{wf} = \frac{g_{\vartheta f}\beta_{\vartheta f}\bar{\zeta}_{\vartheta f}^2 \underline{\zeta}_{\vartheta f}^2 \zeta_{\vartheta f}}{(\bar{\zeta}_{\vartheta f} - \zeta_{\vartheta f})(\zeta_{\vartheta f} + \underline{\zeta}_{\vartheta f})} - \frac{\dot{\beta}_{\vartheta f} e_{\vartheta f}}{\beta_{\vartheta f}} + \frac{1}{d_f}\left(v_f \sin\vartheta_f + \frac{\eta_{2f}^T \Gamma_{2f}}{\varepsilon_f}\right) + \frac{\hat{h}_l}{d_f} \tanh\left(\frac{\Lambda_{\vartheta f}\hat{h}_l}{d_f \beta_{\vartheta f}\sigma_f}\right). \tag{27}$$

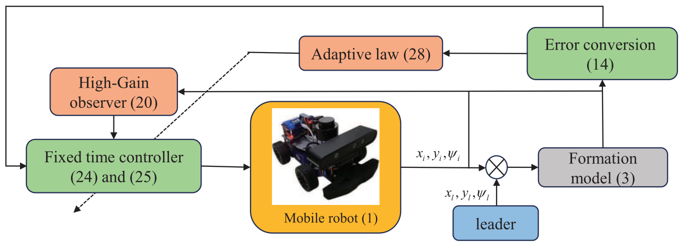

Fig. 2. Controller structure diagram.

The following adaptive law $\hat{h}_l$ is designed as follows:

$$\dot{\hat{h}}_l = \gamma^{-1}\left(\left|\frac{\Lambda_{df}}{\beta_{df}}\right| + \left|\frac{\Lambda_{\vartheta f}}{\beta_{\vartheta f} d_f}\right| - \kappa_i \hat{h}_l\right), \tag{28}$$

where $g_{df} > 0, g_{\vartheta f} > \gamma > 0$ and $\kappa > 0$ are design parameters.

Until now, the design of the control and observer has been fully completed. To gain a more intuitive understanding of the control structure, the following control structure diagram is provided in Fig. 2.

Remark 2. Due to communication denial, the position and speed information of the leader becomes unavailable. Therefore, this study utilizes data collected from onboard sensors to effectively reconstruct the leader's position information. Subsequently, to address the issue of unknown velocity information of the leader, this paper proposes a high gain observer method to achieve real-time estimation of the leader's velocity information. This approach demonstrates higher flexibility and lower conservatism compared to the existing results [9, 11, 14, 15] that only uses speed upper bounds for estimation.

Remark 3. When designing a fixed time controller, traditional methods typically incorporate two terms: one where the exponent of the power function is greater than one (i.e. $z^p, p > 1$), and the other where the exponent is less than one (i.e. $z^q, q < 1$). These two components together form a fixed-time controller, each playing distinct roles. When the error term is less than one, the term with an exponent less than one exhibits a faster decay rate, thus playing a significant role. Conversely, when the error is greater than one, the term with an exponent greater than one assumes a major role. This switching-like mechanism underpins fixed-time control. However, although this traditional fixed-time control strategy ensures reaching a stable state within a predetermined time frame, it also induces substantial oscillations in the control signal. Such high-amplitude oscillations not only challenge the physical components of the system but may also impact the long-term stability and reliability of the system.

In order to solve the problem of large amplitude signal vibration in traditional fixed time controllers, this paper designs a new controller based on the saturation characteristics of tanh function and fixed time control theory. This designed newly controller can effectively reduce the large amplitude vibration of signals in traditional fixed time control, thereby saving energy consumption to a certain extent. Through carefully designed control strategies, it is possible to reduce the oscillation of control signals while maintaining system stability, which is of great significance for improving the response quality and efficiency of the system.

3.3. *Stability analysis*

Theorem 1. *For the multi-UGV system governed by the dynamic model* (2), *the proposed control signals* (24), (25), *synergistically integrated with the high-gain observer* (20) *and adaptive update law* (28), *guarantee that all signals of this multi-UGV system are bounded. Furthermore, the designed control ensures that the conditions for maintaining connectivity and avoiding collisions are not compromised.*

Proof. The Lyapunov function V_i is constructed as

$$V_i = \frac{1}{2}B_{df}^2 + \frac{1}{2}B_{\vartheta f}^2 + \frac{1}{2\gamma}\tilde{h}_l^2, \tag{29}$$

where $B_{jf} = \frac{\bar{\zeta}_{jf}\underline{\zeta}_{jf}\zeta_{jf}}{(\bar{\zeta}_{jf}-\zeta_{jf})(\zeta_{jf}+\underline{\zeta}_{jf})}$, $j = d, \vartheta$. $\bar{\zeta}_{jf}$ and $\underline{\zeta}_{j\vartheta}$ are the designed boundaries of time invariant restricted with $\bar{\zeta}_{jf} < \zeta_{jf} < \underline{\zeta}_{jf}$, $j = d, \vartheta$, and $\tilde{h}_l = \hat{h}_l - h_l$, $\hat{h}_l$ is the estimate h_l.

Taking the derivative of (29) and substituting (22) and (23) into $\dot{V}_i$, one has

$$\begin{aligned}\dot{V}_i = {} & \Lambda_{df}(\zeta_{df})\left[\frac{1}{\beta_{df}}(-v_f\cos\vartheta_f + \dot{p}_l^T\Gamma_{1f}) - \frac{\dot{\beta}_{df}e_{df}}{\beta_{df}^2}\right] \\ & + \Lambda_{\vartheta f}(\zeta_{\vartheta f})\left[\frac{1}{\beta_{\vartheta f}}\left(\frac{1}{d_f}(v_f\sin\vartheta_f + \dot{p}_l^T\Gamma_{2f}) - w_f\right)\right] \\ & + \frac{1}{\gamma}\tilde{h}_l\dot{\hat{h}}_l,\end{aligned} \tag{30}$$

where $\Lambda_{jf} = \frac{\bar{\zeta}_{jf}^2\underline{\zeta}_{jf}^2(\zeta_{jf}^2+\bar{\zeta}_{jf}\underline{\zeta}_{jf})\zeta_{jf}}{(\bar{\zeta}_{jf}-\zeta_{jf})^3(\zeta_{jf}+\underline{\zeta}_{jf})^3}$, $j = d, \vartheta$.

Substituting control signal (24), (25) and adaptive (28) into (30) can be rewritten as

$$\begin{aligned}\dot{V}_i = {} & \frac{-\Lambda_{df}(\zeta_{df})g_{df}\bar{\zeta}_{df}^2\underline{\zeta}_{df}^2\zeta_{df}}{(\bar{\zeta}_{df}-\zeta_{df})(\zeta_{df}+\underline{\zeta}_{df})} - \frac{\Lambda_{\vartheta f}(\zeta_{df})g_{\vartheta f}\bar{\zeta}_{\vartheta f}^2\underline{\zeta}_{\vartheta f}^2\zeta_{\vartheta f}}{(\bar{\zeta}_{\vartheta f}-\zeta_{\vartheta f})(\zeta_{\vartheta f}+\underline{\zeta}_{\vartheta f})} \\ & + \left|\frac{\Lambda_{df}}{\beta_{df}}\right|\hat{h}_l - \frac{\Lambda_{df}\hat{h}_l}{\beta_{df}}\tanh\left(\frac{\Lambda_{df}\hat{h}_l}{\beta_{df}\sigma_f}\right) + \left|\frac{\Lambda_{\vartheta f}}{\beta_{\vartheta f}d_f}\right|\hat{h}_l \\ & - \frac{\Lambda_{\vartheta f}\hat{h}_l}{\beta_{\vartheta f}d_f}\tanh\left(\frac{\Lambda_{\vartheta f}\hat{h}_l}{\beta_{\vartheta f}d_f\sigma_f}\right) + \frac{\Lambda_{df}\varepsilon_f\ddot{\Upsilon}_f\Gamma_{1f}}{\beta_{df}} - h_l\left|\frac{\Lambda_{df}}{\beta_{df}}\right| \\ & + \frac{\Lambda_{\vartheta f}\varepsilon_f\ddot{\Upsilon}_f\Gamma_{2f}}{\beta_{\vartheta f}d_f} - h_l\left|\frac{\Lambda_{\vartheta f}}{\beta_{\vartheta f}d_f}\right| - \kappa_i\tilde{h}_l\hat{h}_l + 2k_p\aleph,\end{aligned} \tag{31}$$

where

$$\frac{-g_{jf}\Lambda_{jf}(\zeta_{jf})\bar{\zeta}_{jf}^2\underline{\zeta}_{jf}^2\zeta_{jf}}{(\bar{\zeta}_{jf}-\zeta_{jf})(\zeta_{jf}+\underline{\zeta}_{jf})} \le g_{jf}\left[\frac{\bar{\zeta}_{jf}\underline{\zeta}_{jf}\zeta_{jf}}{(\bar{\zeta}_{jf}-\zeta_{jf})(\zeta_{jf}+\underline{\zeta}_{jf})}\right]^4. \tag{32}$$

Also, due to the high gain observation parameter $\varepsilon_f < 1$, the following inequality can be obtained

$$\begin{aligned}\frac{\Lambda_{df}\varepsilon_f\ddot{\Upsilon}_f\Gamma_{1f}}{\beta_{df}} & \le \left|\frac{\Lambda_{df}\varepsilon_f\ddot{\Upsilon}_f\Gamma_{1f}}{\beta_{df}}\right| \\ & \le \left|\frac{\Lambda_{df}\varepsilon_f}{\beta_{df}}\right| ||\ddot{\Upsilon}_f|| \le h_l\left|\frac{\Lambda_{df}}{\beta_{df}}\right|,\end{aligned} \tag{33}$$

$$\begin{aligned}\frac{\Lambda_{\vartheta f}\varepsilon_f\ddot{\Upsilon}_f\Gamma_{2f}}{\beta_{\vartheta f}d_f} & \le \left|\frac{\Lambda_{\vartheta f}\varepsilon_f\ddot{\Upsilon}_f\Gamma_{2f}}{\beta_{df}d_f}\right| \\ & \le \left|\frac{\Lambda_{\vartheta f}\varepsilon_f}{\beta_{\vartheta f}d_f}\right| ||\ddot{\Upsilon}_f|| \le h_l\left|\frac{\Lambda_{\vartheta f}}{\beta_{\vartheta f}d_f}\right|.\end{aligned} \tag{34}$$

On the basis of $0 \le |b| - b\tanh(\frac{b}{\delta}) \le k_p\delta, k_p = 0.2785$, and after calculation, it can be concluded that

$$\begin{aligned}\dot{V}_i \le {} & -g_{df}\left[\frac{\bar{\zeta}_{df}\underline{\zeta}_{df}\zeta_{df}}{(\bar{\zeta}_{df}-\zeta_{df})(\zeta_{df}+\underline{\zeta}_{df})}\right]^4 \\ & - g_{\vartheta f}\left[\frac{\bar{\zeta}_{\vartheta f}\underline{\zeta}_{\vartheta f}\zeta_{\vartheta f}}{(\bar{\zeta}_{\vartheta f}-\zeta_{\vartheta f})(\zeta_{\vartheta f}+\underline{\zeta}_{\vartheta f})}\right]^4 \\ & - \kappa_i\tilde{h}_l\hat{h}_l + 2k_p\delta + 2k_p\aleph.\end{aligned} \tag{35}$$

Further, applying the following inequality

$$-\sum_{i=1}^{n}\frac{X_i^2}{l_i} \le -\left(\sum_{i=1}^{n}\frac{X_i^2}{2l_i}\right)^p - \frac{1}{n^{q-1}}\left(\sum_{i=1}^{n}\frac{X_i^2}{2l_i}\right)^q + \varpi, \tag{36}$$

where X_i is a bounded variable satisfying $|X_i| \le \bar{X}_i$ with $\bar{X}_i$ being a positive constant, and $l_i > 0, 0 < p < 1, q > 1, \varpi = (1-p)p^{\frac{p}{1-p}} + \sum_{i=1}^{n}(\frac{\bar{X}_i^2}{2l_i})^q$, one has

$$-\left[\frac{\bar{\zeta}_{df}\underline{\zeta}_{df}\zeta_{df}}{(\bar{\zeta}_{df}-\zeta_{df})(\zeta_{df}+\underline{\zeta}_{df})}\right]^4$$

$$
\begin{aligned}
&\le -\left[\frac{\bar{\zeta}_{df}\underline{\zeta}_{df}\zeta_{df}}{(\bar{\zeta}_{df}-\zeta_{df})(\zeta_{df}+\underline{\zeta}_{df})}\right]^{2p} \\
&\quad + \left[\frac{\bar{\zeta}_{df}\underline{\zeta}_{df}\zeta_{df}}{(\bar{\zeta}_{df}-\zeta_{df})(\zeta_{df}+\underline{\zeta}_{df})}\right]^{2q} + \varpi_1 \\
&\quad -\left[\frac{\bar{\zeta}_{\vartheta f}\underline{\zeta}_{\vartheta f}\zeta_{\vartheta f}}{(\bar{\zeta}_{\vartheta f}-\zeta_{\vartheta f})(\zeta_{\vartheta f}+\underline{\zeta}_{\vartheta f})}\right]^{4} \\
&\le -\left[\frac{\bar{\zeta}_{\vartheta f}\underline{\zeta}_{\vartheta f}\zeta_{\vartheta f}}{(\bar{\zeta}_{\vartheta f}-\zeta_{\vartheta f})(\zeta_{\vartheta f}+\underline{\zeta}_{\vartheta f})}\right]^{2p} \\
&\quad + \left[\frac{\bar{\zeta}_{\vartheta f}\underline{\zeta}_{\vartheta f}\zeta_{\vartheta f}}{(\bar{\zeta}_{\vartheta f}-\zeta_{\vartheta f})(\zeta_{\vartheta f}+\underline{\zeta}_{\vartheta f})}\right]^{2q} + \varpi_2. \qquad (37)
\end{aligned}
$$

Next, using Young's inequality, one can obtain $-\tilde{h}_l\hat{h}_l \le -\frac{1}{2}\tilde{h}_l^2 + \frac{1}{2}h_l^2$, and $-\tilde{h}_l^2 \le -(\frac{1}{2}\tilde{h}_l^2)^p - (\frac{1}{2}\tilde{h}_l^2)^q + \varpi_3$.

After the above calculation, the inequality below can be obtained

$$
\begin{aligned}
\dot{V}_i \le & -g_{df}\left[\left(\frac{\bar{\zeta}_{df}\underline{\zeta}_{df}\zeta_{df}}{(\bar{\zeta}_{df}-\zeta_{df})(\zeta_{df}+\underline{\zeta}_{df})}\right)^2\right]^p \\
& - g_{df}\left[\left(\frac{\bar{\zeta}_{df}\underline{\zeta}_{df}\zeta_{df}}{(\bar{\zeta}_{df}-\zeta_{df})(\zeta_{df}+\underline{\zeta}_{df})}\right)^2\right]^q \\
& - g_{\vartheta f}\left[\left(\frac{\bar{\zeta}_{\vartheta f}\underline{\zeta}_{\vartheta f}\zeta_{\vartheta f}}{(\bar{\zeta}_{\vartheta f}-\zeta_{\vartheta f})(\zeta_{\vartheta f}+\underline{\zeta}_{\vartheta f})}\right)^2\right]^p \\
& - g_{\vartheta f}\left[\left(\frac{\bar{\zeta}_{\vartheta f}\underline{\zeta}_{\vartheta f}\zeta_{\vartheta f}}{(\bar{\zeta}_{\vartheta f}-\zeta_{\vartheta f})(\zeta_{\vartheta f}+\underline{\zeta}_{\vartheta f})}\right)^2\right]^q \\
& - \kappa_i\left(\frac{1}{2}\tilde{h}_l^2\right)^p - \kappa_i\left(\frac{1}{2}\tilde{h}_l^2\right)^q + D_i, \qquad (38)
\end{aligned}
$$

where $D_i = g_{df}\varpi_1 + g_{\vartheta f}\varpi_2 + \varpi_3 + 2k_p\delta$. From the definition of V_i in Eq. (29), the final form of $\dot{V}_i$ can be obtained as follows:

$$\dot{V}_i \le -\hbar_{1i}V_i^p - \hbar_{2i}V_i^q + D_i, \qquad (39)$$

where $\hbar_{1i} = \min\{2^p g_{df}, 2^p g_{\zeta f}, 2^p\gamma^p\kappa_i\}$ and $\hbar_{2i} = \min\times\{2^q g_{df}, 2^q g_{\vartheta f}, 2^p\gamma^q\kappa_i\}$.

The inequality (45) can be rewritten as

$$\dot{V}_i \le -\wp\hbar_{1i}V_i^p - \hbar_{2i}V_i^q - (1-\wp)\hbar_{1i}V_i^p + D_i, \qquad (40)$$

where $0 < \wp < 1$ is a given constant. According to (31), one has $\dot{V}_i \le -\wp\hbar_{1i}V_i^p - \hbar_{2i}V_i^q$, when $V_i^p \ge \frac{D_i}{(1-\wp)\hbar_{1i}}$, which implies that V_i can converges to the set $\Omega_1 = \{V_i\,|\,V_i < (\frac{D_i}{(1-\wp)\hbar_{1i}})^{\frac{1}{p}}\}$. So, we can obtain $\frac{1}{2}B_{df}^2 + \frac{1}{2}B_{\vartheta f}^2 + \frac{1}{2\gamma}\tilde{h}_l^2 \le (\frac{D_i}{(1-\wp)\hbar_{1i}})^{\frac{1}{p}}$, and the result can be obtained

$$|B_{jf}| \le \Delta, \quad j = d, \vartheta, \qquad (41)$$

where $\Delta = \sqrt{2(\frac{D_i}{(1-\wp)\hbar_{1i}})^{\frac{1}{p}}} > 0$ can be taken as a small neighborhood of zero in fixed time, yielding

$$\left|\frac{\bar{\zeta}_{jf}\underline{\zeta}_{jf}\zeta_{jf}}{(\bar{\zeta}_{jf}-\zeta_{jf})(\zeta_{jf}+\underline{\zeta}_{jf})}\right| \le \Delta, \quad j = d, \vartheta \qquad (42)$$

which implies that $\underline{A} \le \zeta_{jf} \le \bar{A}$

$$
\begin{aligned}
\bar{A} &= \frac{\Delta(\bar{\zeta}_{jf}-\underline{\zeta}_{jf}) - \bar{\zeta}_{jf}\underline{\zeta}_{jf} - \sqrt{(-\Delta\bar{\zeta}_{jf}+\bar{\zeta}_{jf}\underline{\zeta}_{jf}+\Delta\underline{\zeta}_{jf})+4\Delta^2\bar{\zeta}_{jf}\underline{\zeta}_{jf}}}{2\Delta}, \\
\underline{A} &= \frac{\Delta(\bar{\zeta}_{jf}-\underline{\zeta}_{jf}) + \bar{\zeta}_{jf}\underline{\zeta}_{jf} - \sqrt{(\Delta\bar{\zeta}_{jf}+\bar{\zeta}_{jf}\underline{\zeta}_{jf}-\Delta\underline{\zeta}_{jf})+4\Delta^2\bar{\zeta}_{jf}\underline{\zeta}_{jf}}}{2\Delta}.
\end{aligned}
$$

So, we can obtain that the formation errors e_{jf} can arrive at the set $\Omega_2 = \{e_{jf}|\underline{A}\beta_{jf} \le e_{jf} \le \bar{A}\beta_{jf}\}$ in fixed time $T = \frac{1}{\wp\hbar_{1i}(1-p)} + \frac{1}{\hbar_{2i}(1-q)}$.

Then by completion of squares, it yields

$$2\sqrt{\hbar_{1i}\hbar_{2i}V_i^{p+q}} \le \hbar_{1i}V_i^p + \hbar_{2i}V_i^q \qquad (43)$$

with $p = 1 + \frac{1}{\varsigma}, q = 1 - \frac{1}{\varsigma}$, so, we can obtain

$$\dot{V}_i \le -\hbar_{1i}V_i^p - \hbar_{2i}V_i^q + D_i \le -2\sqrt{\hbar_{1i}\hbar_{2i}}V_i + D_i \qquad (44)$$

which implies that

$$V_i \le \left(V(0) - \frac{D_i}{2\sqrt{\hbar_{1i}\hbar_{2i}}}\right)e^{(-2\sqrt{\hbar_{1i}\hbar_{2i}}t)} + \frac{D_i}{2\sqrt{\hbar_{1i}\hbar_{2i}}}. \qquad (45)$$

Thus, it follows from (29) that $B_{df}, B_{\vartheta f}$ and $\tilde{h}_l$ are bounded. According to (14), the errors $\zeta_{df}, \zeta_{\vartheta f}, e_{df}$ and $e_{\vartheta f}$ are bounded. In addition, the controllers v_f and w_f are bounded.

Finally, from (29) and (45), we can know that V_i is ultimately bounded by $\frac{D_i}{2\sqrt{\hbar_{1i}\hbar_{2i}}}$ when $t \to \infty$. Similarly, by solving inequalities $B_{jf} \le \sqrt{\frac{D_i}{\sqrt{\hbar_{1i}\hbar_{2i}}}}$, we obtain

$$\underline{\ell} \le \zeta_{jf}(\infty) \le \bar{\ell}, \qquad (46)$$

where

$$
\begin{aligned}
\underline{\ell} &= \frac{\iota_i\bar{\zeta}_{jf} - \iota_i\underline{\zeta}_{jf} + \bar{\zeta}_{jf}\underline{\zeta}_{jf} - \sqrt{(\iota_i\bar{\zeta}_{jf} - \iota_i\underline{\zeta}_{jf} + \bar{\zeta}_{jf}\underline{\zeta}_{\vartheta f})^2 + 4\iota_i^2\bar{\zeta}_{jf}\underline{\zeta}_{jf}}}{2\iota_i}, \\
\bar{\ell} &= \frac{\iota_i\bar{\zeta}_{jf} - \iota_i\underline{\zeta}_{jf} - \bar{\zeta}_{jf}\underline{\zeta}_{jf} + \sqrt{(-\iota_i\bar{\zeta}_{jf} + \iota_i\underline{\zeta}_{jf} + \bar{\zeta}_{jf}\underline{\zeta}_{\vartheta f})^2 + 4\iota_i^2\bar{\zeta}_{jf}\underline{\zeta}_{jf}}}{2\iota_i}
\end{aligned}
$$

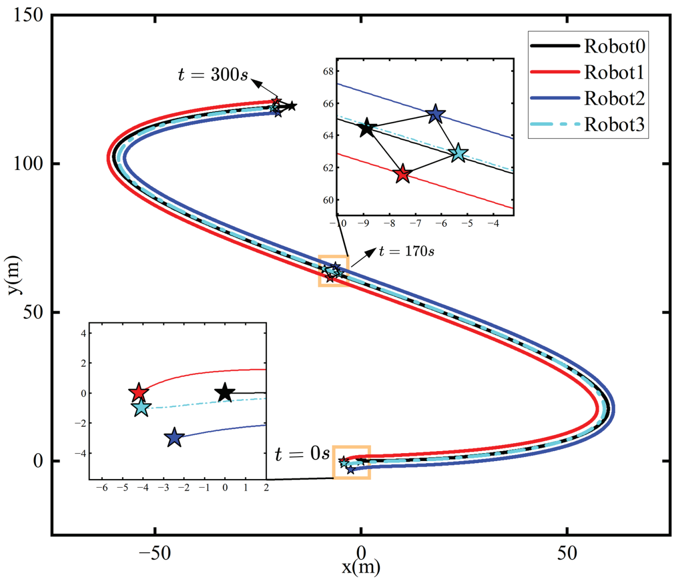

Fig. 3. Trajectory diagram of the phase plane of the mobile robot.

with $\iota_i = \sqrt{\frac{D_i}{\sqrt{\hbar_{1i}\hbar_{2i}}}}$, Therefore, it can be obtained

$$\underline{\ell}\beta_{jf,\infty} \le e_{jf}(\infty) \le \bar{\ell}\beta_{jf,\infty}. \tag{47}$$

So far, all the proof processes have been completed. □

4. Simulation Results

In the section, we use four UGV to verify the effectiveness of the FTFCS. The leader's trajectory is given as follows: $x_l = 60 * \sin(0.02t); y_l = -60 * \cos(0.01t) + 60$. The maximum communication distance is $d_{\max,f} = 5m$, the minimum safety distance is $d_{\min,f} = 3m$ and maximum perception angle is $\vartheta_{\max} = \pi/2$. The desired distances are selected as $d_1^* = d_2^* = 4m, d_3^* = 4.5$, and the desired angles are $\vartheta_1^* = -\pi/6, \vartheta_2^* = \pi/6, \vartheta_3^* = 0$. According to (13), we can easily calculate the performance constraint function

$$\begin{aligned}
\beta_{d1} &= \beta_{d2} = (1-0.1)e^{-0.3t} + 0.1,\\
\beta_{d3} &= (0.5-0.1)e^{-0.3t} + 0.1,\\
\beta_{\vartheta 1} &= (2\pi/3-0.1)e^{-0.3t} + 0.1,\\
\beta_{\vartheta 2} &= (\pi/3-0.1)e^{-0.3t} + 0.1,\\
\beta_{\vartheta 3} &= (\pi/2-0.1)e^{-0.3t} + 0.1.
\end{aligned} \tag{48}$$

The design parameters are as follows: $g_{df} = g_{\vartheta f} = 1, (f = 1, 2, 3), \varepsilon_1 = \varepsilon_2 = \varepsilon_3 = 0.5$, and $\mu_1 = \mu_2 = \mu_3 = 20$. The initial conditions of the four UGVs are given by $q_0 = [0, 0, 0]^T, q_1 = [-4.2, 0, \pi/4]^T, q_2 = [-2.5, -3, 0]^T, q_3 = [-4, -1, -\pi/9]^T$, with $\eta_{1f} = [0, 0]^T, \eta_{2f} = [0, 0]^T$.

The results of the simulation are shown in Figs. 3–16. Figure 3 shows the trajectory of four UGVs moving in the phase plane, indicating that each follower can follow the leader well and maintain the diamond shaped motion. Furthermore, from Figs. 4–6, it is clearly visible that the formation error e_{df} always evolves within the conical envelope of the preset performance, and it can converge to a small neighborhood of zero in fixed time. From Figs. 5 and 6, it

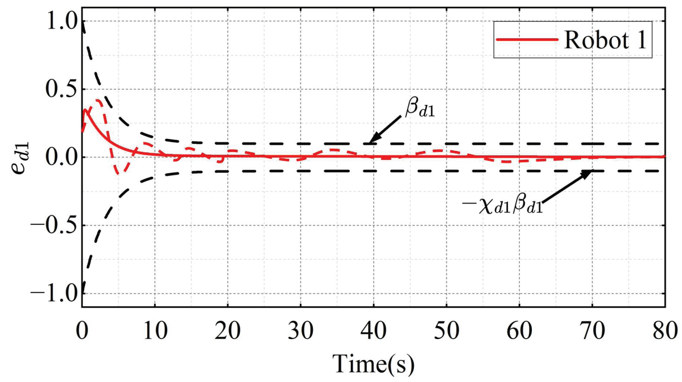

Fig. 4. Relative distance error e_{d1} with the proposed strategy (solid line) and finite-time (dotted line).

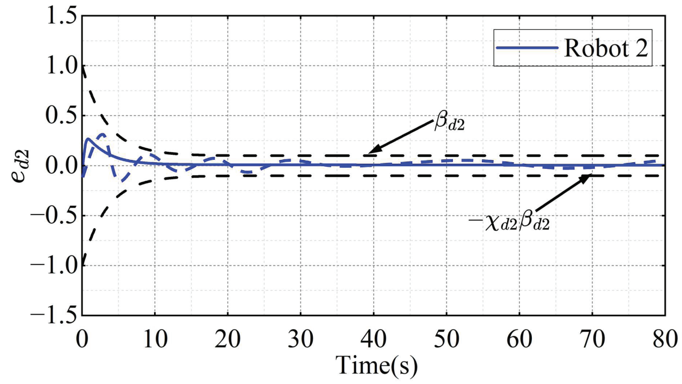

Fig. 5. Relative distance error e_{d2} with the proposed strategy (solid line) and finite-time (dotted line).

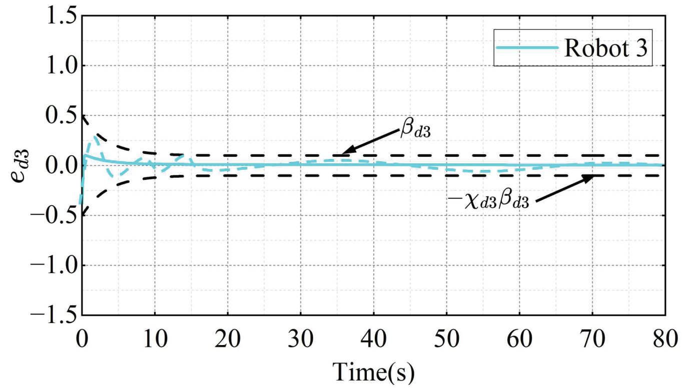

Fig. 6. Relative distance error e_{d3} with the proposed strategy (solid line) and finite-time (dotted line).

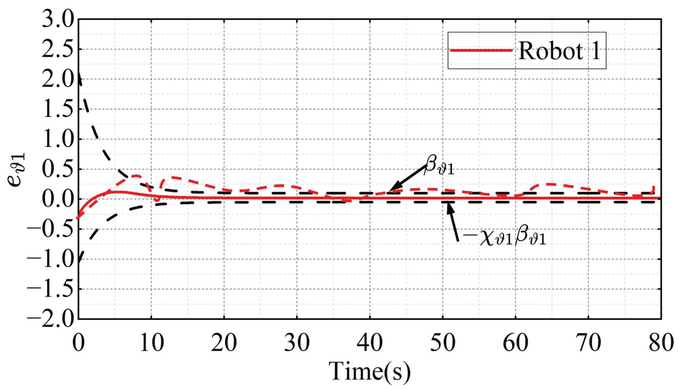

Fig. 7. Bearing angle error $e_{\vartheta 1}$ with the proposed strategy (solid line) and finite-time (dotted line).

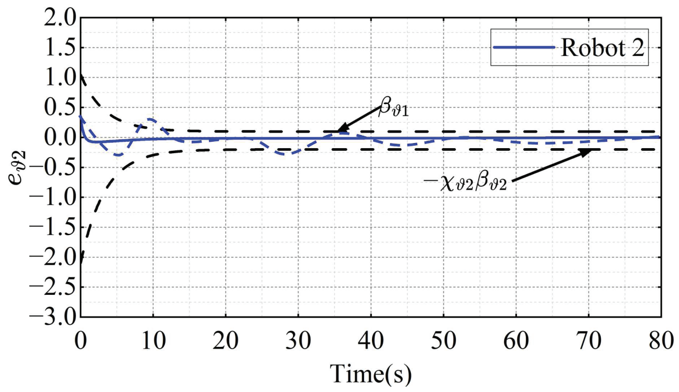

Fig. 8. Bearing angle error $e_{\vartheta 2}$ with the proposed strategy (solid line) and finite-time (dotted line).

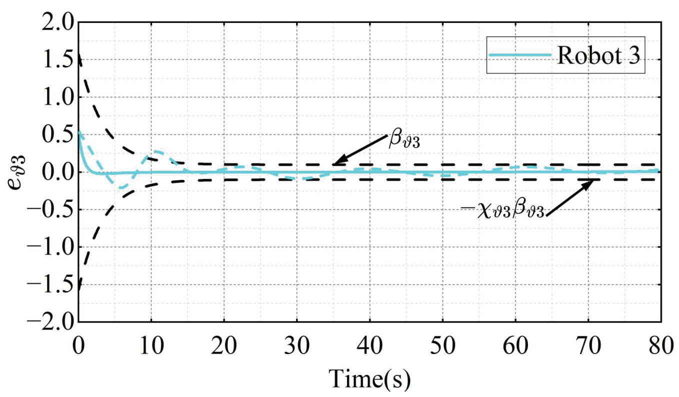

Fig. 9. Bearing angle error $e_{\vartheta 3}$ with the proposed strategy (solid line) and finite-time (dotted line).

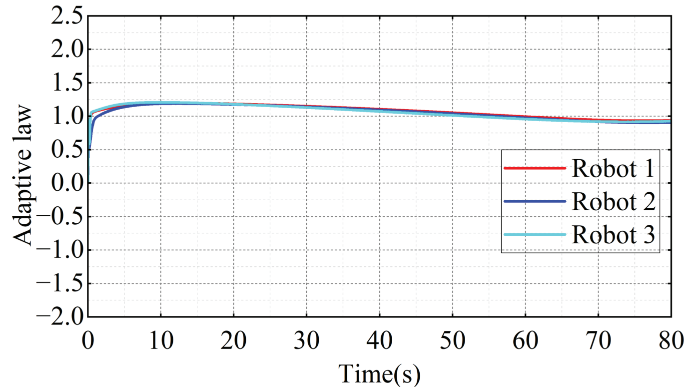

Fig. 10. Adaptive laws $\hat{h}_f$.

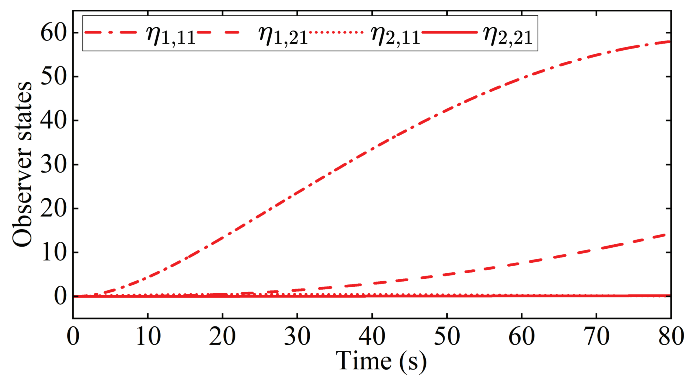

Fig. 11. Observer status of UGV1.

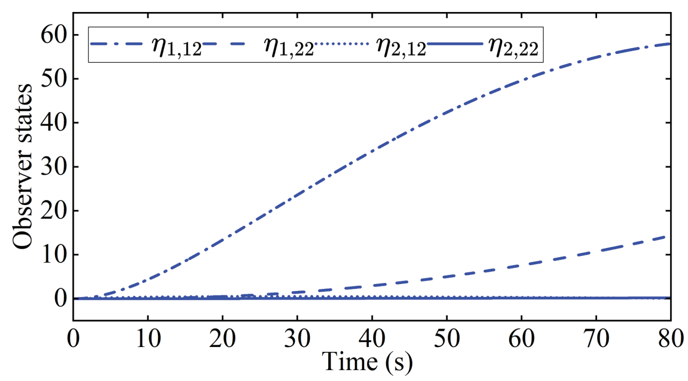

Fig. 12. Observer status of UGV2.

can be seen that due to the different follow-up distances set between each vehicle, the boundaries of the preset performance function are also different. From Figs. 7–9, it can be seen that the relative angular error $e_{\vartheta f}$ can be well approximated by the desired angle to form a formation, and the error will not exceed the pre-set boundary to avoid the occurrence of singularities in the controller. Moreover, since the desired angle for each vehicle is different, the pre-set performance function boundary also takes a non-symmetric form, further demonstrating that the designed controller can handle asymmetric constraint problems. Furthermore, it is clear from the comparison between the solid and dashed lines in the figures that the control algorithm proposed in this paper has better convergence performance compared to finite time

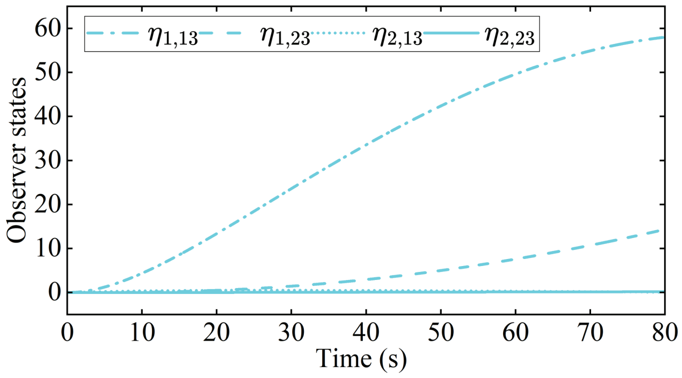

Fig. 13. Observer status of UGV3.

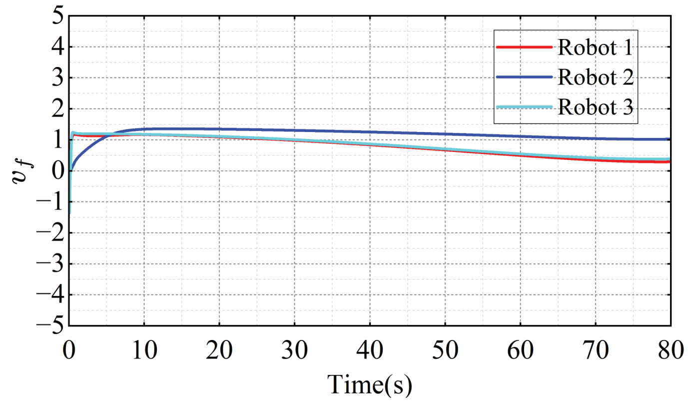

Fig. 14. Control inputs v_f.

formation control. Figure 10 shows the evolution trajectory of the adaptive law $\hat{h}_l$. Figures 11–13 show the state values of the observer system designed for each follower, and it can be clearly seen from the figures that the trend of the observed values is also basically the same. That's because in this simulation, a leader was used to achieve the shape of the diamond formation. The evolution of the control v_f and w_f variables from Figs. 14 and 15 is presented, and it is evident from the figure that the control variables do not exhibit large jumps but are smooth, further confirming the effectiveness of the designed controller.

Remark 4. For finite time, the convergence time of the system is highly sensitive to initial conditions, and different initial conditions may lead to vastly different control effects. The expression of its convergence time can be represented as

$$T \leq \frac{\ln[(\beta_1 V^{1-\varpi}(x_0) + \beta_2)\beta_2]}{\beta_1(1-\varpi)}.$$

It can be clearly seen from the above expression that the convergence time of the system not only strictly depends on the initial conditions x_0 of the system, but also on additional system parameters. Therefore, the selection of finite time control parameters is relatively difficult, as it requires precise system models and in-depth theoretical knowledge. For a fixed time, the convergence time form of the system is

$$T \leq \frac{1}{\hbar_1(p-1)} + \frac{1}{\hbar_2(1-q)}. \tag{49}$$

From the above expression, it is clear that the convergence time of the system does not depend on the initial value, but only on the selection of parameters which further improved the flexibility of the system.

Furthermore, from Fig. 16, it can be easily seen that the new control strategy consumes less energy compared to traditional FTFCS algorithms [17], while keeping the formation time unchanged, which can roughly save 30%. Table 1 gives the absolute value of the normalized tracking error to further

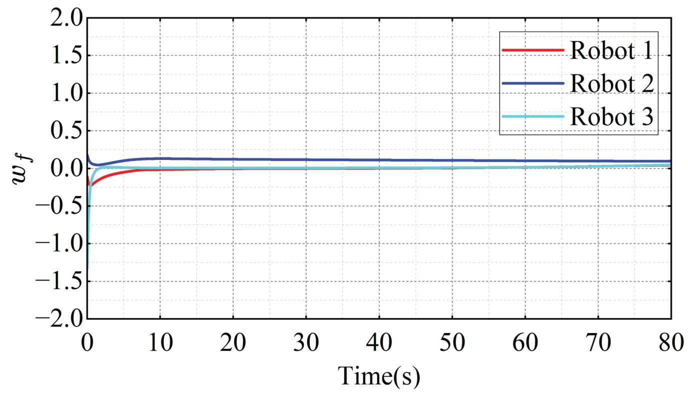

Fig. 15. Control inputs w_f.

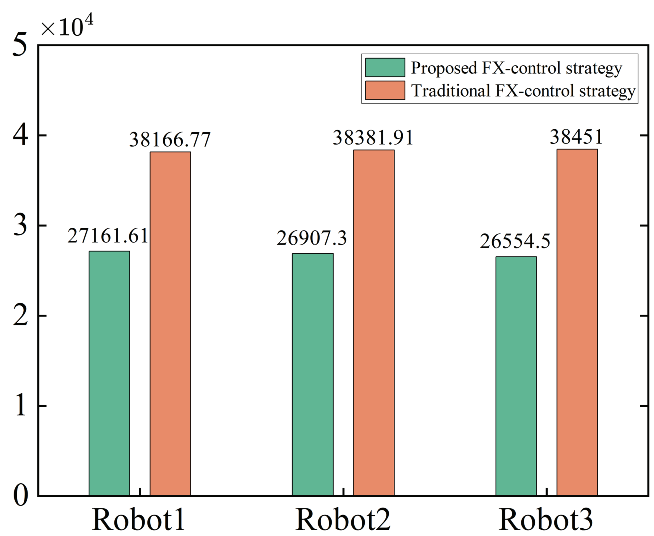

Fig. 16. Comparison of energy to control total input.

Table 1. Performance index values of tracking errors.

Performance index	Proposed method	Method in [17]	Degradation proportion in [17]
$\frac{1}{n}\sum_{i=1}^{m}\lvert e_{d1}\rvert$	0.1701	0.2068	21.15%
$\frac{1}{n}\sum_{i=1}^{m}\lvert e_{d2}\rvert$	0.1627	0.2024	24.40%
$\frac{1}{n}\sum_{i=1}^{m}\lvert e_{d3}\rvert$	0.1721	0.2215	28.70%
$\frac{1}{n}\sum_{i=1}^{m}\lvert e_{\vartheta 1}\rvert$	0.0825	0.1114	35.03%
$\frac{1}{n}\sum_{i=1}^{m}\lvert e_{\vartheta 2}\rvert$	0.0171	0.0249	45.61%
$\frac{1}{n}\sum_{i=1}^{m}\lvert e_{\vartheta 3}\rvert$	0.0635	0.0836	31.65%

verify the effectiveness of the proposed control strategy. It can be seen intuitively from the table that the proposed control strategy also presents a good effect in tracking performance. In conclusion, the proposed control strategy shows good performance in controlling energy consumption and error.

5. Conclusion

In this paper, we propose a novel fixed-time control strategy based on relative information for UGVs under communication denial conditions. Given that the UGV cannot directly obtain the absolute position and heading information of the leader when communication resources are constrained, we utilize data captured by on-board sensors to accurately reconstruct the leader's position and design an observer to estimate the leader's velocity in real time. Furthermore, we consider the perception range limitations of on-board sensors and collision avoidance constraints. By integrating Barrier Lyapunov Functions (BLF), the hyperbolic tangent (tanh) function, and PPC, we develop a novel fixed-time controller. This controller not only guarantees system connectivity and collision avoidance but also significantly suppresses oscillations and reduces energy consumption of the control inputs.

Acknowledgments

This paper is partly supported by National Science Foundation of China under Grants (62033001) and (62403298); in part by Ministry of Education Humanities and Social Science Planning Fund Project of China (23YJAZH081); in part by Jining City Key Research and Development Program Projects of China (2023ZDZP034).

ORCID

Xinhai Zhuang
https://orcid.org/0000-0002-4551-6938
Jingyi Liu
https://orcid.org/0000-0001-6251-6051
Hengyu Li
https://orcid.org/0000-0002-2243-5908
Yueying Wang
https://orcid.org/0000-0001-9737-6765
Jun Luo
https://orcid.org/0000-0003-4475-2338

References

[1] R. Yang, L. Liu and G. Feng, An overview of recent advances in distributed coordination of multi-agent systems, *Unmanned Syst.* **10**(3) (2022) 307–325.
[2] F. Li, Y. S. Ding, M. K. Zhou, K. Hao and L. Chen, An affection-based dynamic leader selection model for formation control in multirobot systems, *IEEE Trans. Syst. Man Cybern. Syst.* **10**(7) (2017) 1217–1228.
[3] A. D. Liu, W.-A. Zhang, L. Yu, H. Yan and R. Zhang, Formation control of multiple mobile robots incorporating an extended state observer and distributed model predictive approach, *IEEE Trans. Syst. Man Cybern. Syst.* **50**(11) (2020) 4587–4597.
[4] X. Yu and L. Liu, Distributed circular formation control of ring networked nonholonomic vehicles, *Automatica* **68** (2016) 92–99.
[5] T. Balch and R. C. Arkin, Behavior-based formation control for multirobot teams, *IEEE Trans. Robot. Automat.* **14**(6) (1998) 926–939.
[6] A. Sadowska *et al.*, A virtual structure approach to formation control of unicycle mobile robots using mutual coupling, *Int. J. Control.* **84**(11) (2011) 1886–1902.
[7] B. H. Wang, J. Dasdemir, B. Zhang, W. Chen and Z. Zhang, Leader-follower consensus of multivehicle wirelessly networked uncertain systems subject to nonlinear dynamics and actuator fault, *IEEE Trans. Autom. Sci. Eng.* **15**(2) (2018) 492–505.
[8] C. R. He and J. Huang, Leader-following formation tracking for multiple quadrotor helicopters over switching networks, *Unmanned Syst.* **12**(4) (2024) 775–786.
[9] Z. Wang, L. Wang, H. Zhang, L. Vlacic and Q. Chen, Distributed formation control of nonholonomic wheeled mobile robots subject to longitudinal slippage constraints, *IEEE Trans. Syst. Man Cybern. Syst.* **51**(5) (2021) 2992–3003.
[10] D. B. Shen, W. J. Sun and Z. D. Sun, Adaptive PID formation control of nonholonomic robots without leader's velocity information, *ISA Trans.* **53**(2) (2014) 474–480.
[11] Y. Li, S. Dong, K. Li and S. Tong, Fuzzy adaptive fault tolerant time-varying formation control for nonholonomic multirobot systems with range constraints, *IEEE Trans. Intell. Veh.* **8**(6) (2023) 3668–3679.
[12] Y. Yang, Q. Liu, H. Tan, Z. Shen and D. Wu, Collision-free and connectivity-preserving formation control of nonlinear multi-agent systems with external disturbances, *IEEE Trans. Veh. Technol.* **72**(8) (2023) 9956–9968.
[13] H. Wang, W. Liu and M. Tong, Adaptive fuzzy fast finite-time output-feedback tracking control for switched nonlinear systems with full-state constraints, *IEEE Trans. Fuzzy Syst.* **32**(3) (2024) 958–968.
[14] Y. Li, S. Dong and K. Li, Fuzzy adaptive finite-time event-triggered control of time-varying formation for nonholonomic multirobot systems, *IEEE Trans. Intelli. Veh.* **9**(1) (2024) 725–737.
[15] S. -L. Dai, K. Lu and J. Fu, Adaptive finite-time tracking control of nonholonomic multirobot formation systems with limited field-of-view sensors, *IEEE Trans. Cybern.* **52**(10) (2022) 10695–10708.
[16] A. Polyakov, Nonlinear feedback design for fixed-time stabilization of linear control systems, *IEEE Trans. Autom. Control* **57**(8) (2012) 2106–2110.

[17] S. -L. Dai, K. Lu and X. Jin, Fixed-time formation control of unicycle-type mobile robots with visibility and performance constraints, *IEEE Trans. Ind. Electron.* **68**(12) (2021) 12615–12625.

[18] J. Zhang, F. Xu, X. Liu, S. Gu and H. Geng, Fixed-time dynamic surface control for pneumatic manipulator system with unknown disturbances, *IEEE Robot. Automat. Lett.* **7**(4) (2022) 10890–10897.

[19] Z. Lv, Y. Wu, X.-M. Sun and Q.-G. Wang, Fixed-time control for a quadrotor with a cable-suspended load, *IEEE Trans. Intell. Transp. Syst.* **23**(11) (2022) 21932–21943.

[20] J. Zhang, S. Yu and Y. Yan, Fixed-time output feedback trajectory tracking control of marine surface vessels subject to unknown external disturbances and uncertainties, *ISA Trans.* **93** (2019) 145–155.

[21] Y. Li, S. Dong and K. Li, Fixed-time command filter fuzzy adaptive formation control for nonholonomic multirobot systems with unknown dead-ones, *IEEE Trans. Intelli. Transp. Syst.* **25**(11) (2024) 17305–17316.

[22] Y. Wang, X. Liu, Z. Wu and C. Dang, Distributed prescribed-time formation control for underactuated surface vehicles with input saturation: theory and experiment, *IEEE Trans. Intelli. Transp. Syst.* **25**(11) (2024) 18611–18623.

[23] S. -L. Dai, S. He, X. Chen and X. Jin, Adaptive leader-follower formation control of nonholonomic mobile robots with prescribed transient and steady-state performance, *IEEE Trans. Ind. Inform.* **16**(6) (2020) 3662–3671.

[24] Z. Peng, G. Wen, A. Rahmani and Y. Yu, Distributed consensus-based formation control for multiple nonholonomic mobile robots with a specified reference trajectory, *Int. J. Syst. Sci.* **46**(8) (2015) 1–11.

[25] X. Chu, Z. Peng, G. Wen and A. Rahmani, Distributed fixed-time formation tracking of multi-robot systems with nonholonomic constraints, *Neurocomputing* **313** (2018) 167–174.

[26] D. Liang, C. Wang, X. Cai, Y. Li and Y. Xu, Distributed fixed-time leader-following consensus tracking control for nonholonomic multi-agent systems with dynamic uncertainties, *Neurocomputing* **430** (2021) 112–120.

[27] K. Lu, S. Dai and X. Jin, Fixed-Time Rigidity-based formation maneuvering for nonholonomic multirobot systems with prescribed performance, *IEEE Trans. Cybern.* **54**(4) (2022) 2129–2141.

[28] S. Behtash, Robust output tracking for non-linear systems, *Internat. J. Control.* **51**(6) (1990) 1381–1407.

Xinhai Zhuang received B.S. degree in Electronic Information Science and Technology from the Shandong University of Technology in 2020 and M.S. degree in Control Engineering from the Linyi University. He is currently pursuing Ph.D. degree in Mechanical Engineering with Shanghai University, Shanghai, China. His current research interests include robot formation control, fuzzy control, reinforcement learning and swarm intelligence.

Jingyi Liu received B.S. degree in Mechanical Engineering and Automation, M.S. degree and Ph.D. degree in Mechatronic Engineering from the Shanghai University, Shanghai, China, in 2014, 2017 and 2022, respectively, where he is currently Postdoctoral Fellow with the School of Mechatronic Engineering and Automation. His research interests include computer vision, machine learning, automation control, and perception for mobile robotics.

Hengyu Li received B.S. degree in Mechanical Engineering and Automation from the Henan Polytechnic University, China, in 2006, and M.S. and Ph.D. degrees in Mechanical and Electronic Engineering from the Shanghai University, China, in 2009 and 2012, respectively, where he is currently Professor with the School of Mechatronic Engineering and Automation. His research interests include mechatronics and robot bionic vision systems and autonomous cooperative control for multiple robots.

Yueying Wang received B.S. degree in Mechanical Engineering and Automation from the Beijing Institute of Technology, Beijing, China, in 2006, M.S. degree in navigation, guidance, and control and Ph.D. degree in Control Science and Engineering from the Shanghai Jiao Tong University, Shanghai, China, in 2010 and 2015, respectively. He is currently Full Professor with the School of Mechatronic Engineering and Automation, Shanghai University, Shanghai. His research interests include Intelligent perception, control, and decision making of complex dynamic systems, and USVs. Prof. Wang is Associate Editor for IEEE Transactions on Cybernetics, IET-Electronics Letters.

Jun Luo is Director of State Key Laboratory of Mechanical Transmission with Chongqing University, and he is Professor in the School of Mechatronic Engineering and Automation of Shanghai University, China. He received B.S. degree in Mechanical Engineering from the Henan Polytechnic University, Jiaozuo, China, in 1994, M.S. degree in Mechanical Engineering from Henan Polytechnic University, Jiaozuo, China, in 1997, and Ph.D. degree in Research Institute of Robotics in Shanghai Jiao Tong University, Shanghai, China, in 2000. His research areas include robot sensing, sensory feedback, mechatronics, man-machine interfaces, and special robotics.